Histol Histopathol (2019) 34: 1255-1268

http://www.hh.um.es

Histology and Histopathology

From Cell Biology to Tissue Engineering

A sexy approach to pacemaking: differences in function and molecular make up of the sinoatrial node

Ursula Doris[1], Sanjay Kharche[1,2], Maria Petkova[1], Balint Borbas[1], Sunil Jit R.J. Logantha[1], Olga Fedorenko[3,4], Michal Maczewski[5], Urszula Mackiewicz[4], Yu Zhang[1], Anwar Chahal[6,7], Alicia D'Souza[1], Andrew J. Atkinson[1], Halina Dobrzynski[1#] and Joseph Yanni[1#]

[1]Cardiovascular Sciences, Faculty of Biology, Medicine and Health, University of Manchester, Manchester, England, [2]Department of Biophysics and Lawson Health Research Institute, University of Western Ontario, London, Canada, [3]Mental Health Research Institute, Tomsk National Research Medical Centre, [4]School of Non-Destructive Testing and Security, National Tomsk Polytechnic University, Tomsk, Russian Federation, [5]Medical Centre of Postgraduate Education, Warsaw, Poland, [6]Mayo Clinic, Rochester, Minnesota, USA and [7]Papworth Hospital NHS Trust, Cambridge, UK

[#]Contributed equally

Summary. Background. Functional properties of the sinoatrial node (SAN) are known to differ between sexes. Women have higher resting and intrinsic heart rates. Sex determines the risk of developing certain arrhythmias such as sick sinus syndrome, which occur more often in women. We believe that a major contributor to these differences is in gender specific ion channel expression.

Methods. qPCR was used to compare ion channel gene expression in the SAN and right atrium (RA) between male and female rats. Histology, immunohistochemistry and signal intensity analysis were used to locate the SAN and determine abundance of ion channels. The effect of nifedipine on extracellular potential recording was used to determine differences in beating rate between sexes.

Results. mRNAs for $Ca_v1.3$, $K_{ir}3.1$, and Nkx2-5, as well as expression of the L-Type Ca^{2+} channel protein, were higher in the female SAN. Females had significantly higher intrinsic heart rates and the effect of nifedipine on isolated SAN preparations was significantly greater in male SAN. Computer modelling using a SAN cell model demonstrated a higher propensity of pacemaker-related arrhythmias in females.

Conclusion. This study has identified key differences in the expression of $Ca_v1.3$, $K_{ir}3.1$ and Nkx2-5 at mRNA and/or protein levels between male and female SAN. $Ca_v1.3$ plays an important role in the pacemaker function of the SAN, therefore the higher intrinsic heart rate of the female SAN could be caused by the higher expression of $Ca_v1.3$. The differences identified in this study advance our understanding of sex differences in cardiac electrophysiology and arrhythmias.

Key words: Ion channels, Arrhythmias, Pacemaker of the heart, Sinoatrial, Gender, Electrophysiology, Computer modelling

Offprint requests to: Halina Dobrzynski, CTF Building, 46 Grafton Street, Manchester, M13 9NT, England, UK. e-mail: halina.dobrzynski@manchester.ac.uk

DOI: 10.14670/HH-18-115

Introduction

The sinoatrial node (SAN) is the primary pacemaker of the heart and the origin of depolarization (Dobrzynski et al., 2013). Evidence shows that SAN function differs according to sex; males have a slower resting and intrinsic heart rate due to a longer corrected SAN recovery time and atrial refractory period (Burke et al., 1996; Taneja et al., 2001; Peters and Gold, 2004; Sanjeev and Karpawich, 2005). Sick Sinus Syndrome (SSS) is when action potential (AP) generation is dysfunctional within the SAN, hindering electrical wave propagation to the surrounding atrial muscle. SSS symptoms are sinus bradycardia, sinus arrest, and SAN exit block (Rubenstein et al., 1972; Kharche et al., 2017). Sex may be a risk factor for SSS with studies reporting a higher prevalence in females, although

underlying mechanisms are unknown (Nowak et al., 2010; Tadros et al., 2014). Since ion channels are responsible for AP generation, sex-specific differences in the expression and function of ion channels are potential major contributors to the higher prevalence of SSS in females.

The 'funny' current (I_f) plays an important role in the slow spontaneous diastolic depolarization in SAN cardiomyocytes. The inward calcium (Ca^{2+}) currents: L-type and T-type Ca^{2+} currents ($I_{Ca,L}$ and $I_{Ca,T}$), are responsible for the upstroke of the SAN AP and also contribute to the later phase of the diastolic depolarization. $Ca_v1.2$ and $Ca_v1.3$ are responsible for $I_{Ca,L}$ and $Ca_v3.1$ is key ion channel responsible for $I_{Ca,T}$ (Mesirca et al., 2015). Various outward potassium (K^+) currents contribute to repolarisation; the transient outward current (I_{to}) causes the initial rapid repolarisation phase (Lakatta and Sollott, 2002). Further repolarisation is due to three known delayed rectifier K^+ currents: ultra-rapid ($I_{K,ur}$), rapid ($I_{K,r}$) and slow ($I_{K,s}$), generated by: $K_v1.5$, ether-a-go-go-related gene (ERG), and K_vLQT1 respectively (Chandler et al., 2009; Dobrzynski et al., 2013). The muscarinic K^+ current, $I_{K,Ach}$, is composed of the channel subunits: $K_{ir}3.1$ and $K_{ir}3.4$ (Dobrzynski et al., 2001). Acetylcholine activates $I_{K,Ach}$, which slows spontaneous activity of the SAN, thereby decreasing heart rate (Dobrzynski et al., 2001). Intracellular Ca^{2+} also plays an important role in pacemaking and this is achieved through localised Ca^{2+} release from the sarcoplasmic reticulum (SR) via the type 2 ryanodine receptor (RyR2) (Dobrzynski et al., 2013).

This study's aim was to determine whether a difference existed in intrinsic heart rates between male and female SAN, and quantify the ion channel molecular substrates responsible for functional differences.

Materials and methods

Dissection of the SAN from rats for qPCR, histology, immunohistochemistry and functional experiments

Tyrode solution was prepared freshly before dissection. To one litre of molecular water, the following was added: 7 g/L sodium chloride, 0.3 g/L potassium chloride, 0.32 g/L magnesium sulphate, 0.19 g/L sodium phosphate, 2.1 g/L hydrogen carbonate, and 2 g/L glucose. This solution was mixed with an electromagnetic mixer. Oxygen was then bubbled through the solution for 15 minutes to lower the pH to 7.4. 1.8 ml/L calcium chloride was added at this point.

Male and female rats weighing 250-300 g were euthanized through exposure to carbon dioxide in a rising concentration, followed by dislocation of the neck. This method is in compliance with the ethical standards of the University of Manchester and the UK Home Office Animals (Scientific 17 Procedures) Act 1986. The right atria, containing the SAN, were dissected from the hearts using Tyrode's solution.

RNA isolation

Intact SAN preparations were dissected from the heart as previously described (Dobrzynski et al., 2001). Tissue samples (approximately 1×1 mm) were taken from the centre of the SAN as well as the right atrial free wall. The samples were taken approximately at the level of the leading pacemaker site in the SAN (at the level of the main branch from the crista terminalis). The samples were frozen in liquid N_2. Total RNA isolation was performed on these samples with Qiagen RNeasy micro spin columns. 100 ng of total RNA was reversed transcribed with superscript III reverse transcriptase (Invitrogen) using random hexamer priming to produce cDNA.

qPCR

Ion channel gene expression was measured through quantitative PCR (qPCR) n=12 (n=6 from female SAN and atrial muscle and n=6 from male SAN and atrial muscle). All results are given as mean±SEM. Differences were evaluated by t-test with SigmaStat software. Differences were considered significant at the level of $P<0.05$. qPCR was performed using an Applied Biosystems 7900HT instrument, with low density Taqman array cards (Table 1). Expression levels were calculated using the ΔCt method. GAPDH was used as a house keeper/reference transcript.

With the ΔCt method, the abundance of a transcript of interest was normalised to the abundance of the reference transcript to correct for variations in input RNA. The ΔCt method allows the abundance of different transcripts to be roughly compared (as well as the abundance of the transcript of interest in different tissues and age groups). However, the efficiency of the reverse transcription (described above) for different transcripts can vary up to 10× and, therefore, only ≥10× differences in the abundance of different cDNAs (corresponding to different mRNAs) were interpreted as differences in the corresponding mRNAs. Data obtained with the ΔCt method are listed in Table 2.

Carbachol and nifedipine

The rats' SAN preparations in the recording chamber were continuously perfused with Tyrode solution at a rate of 10 ml/minute for 30 minutes to allow the tissue to adjust and to record the baseline beating rate in SAN preparations. 0.1 μM of carbachol or 5 μM of nifedipine was then run over the preparations for 30 minutes. The preparations were then washed with normal Tyrode solution for another 30 minutes and the recovery of the beating rate was recorded, resulting in a total recording time of 90 minutes per preparation. The extracellular potentials were monitored through two stainless steel needles (JcM health) and the measurements were recorded using LabChart software (ADInstruments) as described by Morris et al. (2013). This method was

replicated with 5 μM of nifedipine replacing the 0.1 μM of carbachol. The trace recordings of the baseline beating rate in SAN preparations could be observed in the Chart View window of the LabChart software. The final five minutes of the baseline beating rate in each 90-minute trace recording was selected. The ECG settings

Table 1. Details of assays used on Taqman low-density array cards.

Gene Symbol	Gene Name	Accession Number	Assay ID
Scn4a	sodium channel, voltage-gated, type IV, alpha polypeptide	NM_013178	Rn00565973_m1
Cacna1g	calcium channel, voltage-dependent, T type, alpha 1G subunit	NM_031601.3	Rn00581051_m1
Itpr3	inositol 1, 4, 5-triphosphate receptor 3	NM_013138	Rn00565664_m1
Cacnb3	calcium channel, voltage-dependent, beta 3 subunit	NM_012828	Rn00432233_m1
Kcna2	potassium voltage-gated channel, shaker-related subfamily, member 2	NM_012970	Rn00564239_m1
Scn2b	sodium channel, voltage-gated, type II, beta polypeptide	NM_012877	Rn00563554_m1
Slc4a9	solute carrier family 4, sodium bicarbonate cotransporter, member 9	NM_152938	Rn00596175_m1
Kcnab1	potassium voltage-gated channel, shaker-related subfamily, beta member 1	NM_017303	Rn00568877_m1
Des	Desmin	NM_022531	Rn00574732_m1
Adrb1	adrenergic receptor, beta 1	NM_012701	Rn00824536_s1
18S	Eukaryotic 18S rRNA	N/A	18S
Itpr2	inositol 1,4,5-triphosphate receptor 2	NM_031046	Rn00579067_m1
Atp1a2	ATPase, Na+/K+ transporting, alpha 2 polypeptide	NM_012505	Rn00560789_m1
Tgfb1	transforming growth factor, beta 1	NM_021578	Rn00572010_m1
Kcnk2	potassium channel, subfamily K, member 2	NM_172042	Rn00597042_m1
Kcnd3	potassium voltage gated channel, Shal-related family, member 3	NM_031739	Rn00709608_m1
Slc4a10	solute carrier family 4, sodium bicarbonate transporter-like, member 10	NM_178092	Rn00710136_m1
Kcnj3	potassium inwardly-rectifying channel, subfamily J, member 3	NM_031610	Rn00434617_m1
Cacng7	calcium channel, voltage-dependent, gamma subunit 7	NM_080695	Rn00519216_m1
Kcnd2	potassium voltage gated channel, Shal-related family, member 2	NM_031730	Rn00581941_m1
Hcn3	hyperpolarization-activated cyclic nucleotide-gated potassium channel 3	NM_053685	Rn00586666_m1
Clcn2	chloride channel 2	NM_017137	Rn00567553_m1
Slc4a4	solute carrier family 4, member 4	NM_053424	Rn00584747_m1
Pias3	protein inhibitor of activated STAT 3	NM_031784	Rn00582371_m1
Trpc4	transient receptor potential cation channel, subfamily C, member 4	NM_080396	Rn00584835_m1
Atp1a1	ATPase, Na+/K+ transporting, alpha 1 polypeptide	NM_012504	Rn00560766_m1
Trpc6	transient receptor potential cation channel, subfamily C, member 6	NM_053559	Rn00585635_m1
Cacna2d2	calcium channel, voltage-dependent, alpha 2/delta subunit 2	NM_175592	Rn00457825_m1
Slc4a7	solute carrier family 4, sodium bicarbonate cotransporter, member 7	NM_058211	Rn00589539_m1
Kcnn1	potassium intermediate/small conductance calcium-activated channel, subfamily N, member 1	NM_019313	Rn00570904_m1
Kcnab3	potassium voltage gated channel, shaker related subfamily, beta member 3	NM_031652	Rn00581323_m1
Adora1	adenosine A1 receptor	NM_017155	Rn00567668_m1
Scn5a	sodium channel, voltage-gated, type V, alpha	NM_013125	Rn00565502_m1
Kcnh1	potassium voltage-gated channel, subfamily H (eag-related), member 1	NM_031742	Rn00582012_m1
Kcnj8	potassium inwardly-rectifying channel, subfamily J, member 8	NM_017099	Rn00567317_m1
Cacna2d1	calcium channel, voltage-dependent, alpha2/delta subunit 1	NM_012919	Rn00563853_m1
Myh6	myosin, heavy polypeptide 6, cardiac muscle, alpha	NM_017239	Rn00568304_m1
Cacna2d3	calcium channel, voltage-dependent, alpha 2/delta 3 subunit	NM_175595	Rn00598241_m1
Scn1a	sodium channel, voltage-gated, type 1, alpha polypeptide	NM_030875	Rn00578439_m1
Adra1b	adrenergic receptor, alpha 1b	NM_016991	Rn01471343_m1
Scn3b	sodium channel, voltage-gated, type III, beta	NM_139097	Rn00594710_m1
Cacna1e	calcium channel, voltage-dependent, L type, alpha 1E subunit	NM_019294	Rn00494444_m1
Casq2	calsequestrin 2	NM_017131	Rn00567508_m1
Nkx2-5	NK2 transcription factor related, locus 5 (Drosophila)	NM_053651	Rn00586428_m1
Abcc9	ATP-binding cassette, sub-family C (CFTR/MRP), member 9	NM_013040	Rn00564842_m1
Scn1b	sodium channel, voltage-gated, type I, beta polypeptide	NM_017288	Rn00441210_m1
Trpc2	transient receptor potential cation channel, subfamily C, member 2	NM_022638	Rn00575304_m1
Cdkn2a	cyclin-dependent kinase inhibitor 2A	NM_031550	Rn00580664_m1
Kcnn2	potassium intermediate/small conductance calcium-activated channel, subfamily N, member 2	NM_019314	Rn00570910_m1
Cacna1d	calcium channel, voltage-dependent, L type, alpha 1D subunit	NM_017298	Rn00568820_m1
Atp2a2	ATPase, Ca++ transporting, cardiac muscle, slow twitch 2	NM_017290	Rn00568762_m1
Kcne4	minK-related peptide 3	NM_212526	Rn01769979_s1
Slc16a3	monocarboxylate transporter	NM_030834	Rn00578115_m1
Kcnn3	potassium intermediate/small conductance calcium-activated channel, subfamily N, member 3	NM_019315	Rn00570912_m1
Cacnb1	calcium channel, voltage-dependent, beta 1 subunit	NM_017346	Rn00569267_m1
Atp2b1	ATPase, Ca++ transporting, plasma membrane 1	NM_053311	Rn00584038_m1
Hcn1	hyperpolarization-activated, cyclic nucleotide-gated potassium channel 1	NM_053375	Rn00584498_m1
Kcne3	potassium voltage-gated channel, Isk-related subfamily, member 3	AJ271742	Rn00573728_m1
Kcnh2	potassium voltage-gated channel, subfamily H (eag-related), member 2	NM_053949	Rn00588515_m1
Hcn2	hyperpolarization activated cyclic nucleotide-gated potassium channel 2	NM_053684	Rn01408575_gH

tab was then selected and the cycle length values were measured.

Cryosectioning of SAN preparations

Optimal cutting temperature (OCT) compound was poured over the rat SAN preparations. Isopentane, cooled in liquid nitrogen, was then poured over the OCT coated SAN preparations to freeze the OCT. The SAN preparations were attached to the cryostat chuck using OCT. The frozen SAN preparations were subsequently cryosectioned using the microtome portion of the cryostat with a set thickness of 20µm. The SAN preparations were cut laterally through the superior vena cava, the sectioning then proceeded towards the inferior vena cava. CT (chamber temperature) was kept at -19°C and OT (object temperature) was kept at -17°C. The sections were picked up on SuperFrost Plus slides, 3-4 sections per slide, and stored at -80°C until use. The slides were used for histology and immunohistochemistry.

Histology

Masson's trichrome stains the nuclei dark blue, the cardiomyocytes pink, and the connective tissue blue. The first of the cryosection slides from each SAN preparation, and every subsequent third slide was selected for Masson's trichrome staining; this was to determine the location of the SAN within the preparations. The slides were fixed in Bouin's fluid for 30 minutes in a fume cupboard. The slides were then washed in 70% alcohol for 10 minutes, thrice. The slides were then stained with celestine blue for 10 minutes, then rinsed with distilled water for 5 minutes. The slides were stained with Mayer's haematoxylin for 5 minutes then washed with distilled water for 15 minutes. The slides were stained with acid fuchsin for 5 minutes, then washed with distilled water for 30 minutes. The slides were stained with phosphomolybdic acid for 5 minutes, then drained. The slides were then stained with methyl blue for 1 minute, then washed with distilled water for 20 minutes. Next the slides were dehydrated with 70%

Table 1. continued.

Gene Symbol	Gene Name	Accession Number	Assay ID
Kcna5	potassium voltage-gated channel, shaker-related subfamily, member 5	NM_012972	Rn00564245_s1
Slc4a2	solute carrier family 4, member 2	NM_017048	Rn00566910_m1
Trpc3	transient receptor potential cation channel, subfamily C, member 3	NM_021771	Rn00572928_m1
Adrb3	adrenergic receptor, beta 3	NM_013108	Rn00565393_m1
Kcnk4	potassium channel, subfamily K, member 4	NM_053804	Rn00587450_m1
Gja5	gap junction membrane channel protein alpha 5	NM_019280	Rn00570632_m1
Slc4a3	solute carrier family 4, member 3	NM_017049	Rn00436642_m1
Cacng4	calcium channel, voltage-dependent, gamma subunit 4	NM_080692	Rn00589903_m1
Adra1a	adrenergic receptor, alpha 1a	NM_017191	Rn00567876_m1
Scn9a	sodium channel, voltage-gated, type 9, alpha polypeptide	NM_133289	Rn00591020_m1
Trpc1	transient receptor potential cation channel, subfamily C, member 1	NM_053558	Rn00585625_m1
Myh7	myosin, heavy polypeptide 7, cardiac muscle, beta	NM_017240	Rn00568328_m1
Atp1a3	ATPase, Na+/K+ transporting, alpha 3 polypeptide	NM_012506	Rn00560813_m1
Itpr1	inositol 1,4,5-triphosphate receptor 1	NM_001007235	Rn01425738_m1
Gata4	GATA binding protein 4	NM_144730	Rn00595169_m1
Atp1b1	ATPase, Na+/K+ transporting, beta 1 polypeptide	NM_013113	Rn00565405_m1
Hcn4	hyperpolarization-activated, cyclic nucleotide-gated K+ 4	NM_021658	Rn00572232_m1
Kcnq1	potassium voltage-gated channel, subfamily Q, member 1	NM_032073	Rn00583376_m1
Slc16a1	solute carrier family 16 (monocarboxylic acid transporters), member 1	NM_012716	Rn00562332_m1
Adra1d	adrenergic receptor, alpha 1d	NM_024483	Rn00577931_m1
Slc8a1	solute carrier family 8 (sodium/calcium exchanger), member 1	NM_019268	Rn00570527_m1
Kcnk3	potassium channel, subfamily K, member 3	NM_033376	Rn00583727_m1
Kcnab2	potassium voltage-gated channel, shaker-related subfamily, beta member 2	NM_017304	Rn00568891_m1
Kcnk6	potassium channel, subfamily K, member 6	NM_053806	Rn00821542_g1
Cacnb2	calcium channel, voltage-dependent, beta 2 subunit	NM_053851	Rn00587789_m1
Slc9a1	solute carrier family 9 (sodium/hydrogen exchanger), member 1	NM_012652	Rn00561924_m1
Cacng5	calcium channel, voltage-dependent, gamma subunit 5	NM_080693.1	Rn00589905_m1
Scn8a	sodium channel, voltage-gated, type 8, alpha polypeptide	NM_019266	Rn00570506_m1
Scn3a	sodium channel, voltage-gated, type III, alpha polypeptide	NM_013119	Rn00565438_m1
Gapdh	glyceraldehyde-3-phosphate dehydrogenase	NM_017008.3	Rn99999916_s1
Trpc5	transient receptor protein 5	NM_080898	Rn00590142_m1
Kcnj2	potassium inwardly-rectifying channel, subfamily J, member 2	NM_017296	Rn00568808_s1
Slc4a1	solute carrier family 4, member 1	NM_012651	Rn00561909_m1
Adrb2	adrenergic receptor, beta 2	NM_012492	Rn00560650_s1
Kcnb1	potassium voltage gated channel, Shab-related subfamily, member 1	NM_013186	Rn00755102_m1
Cacna1c	calcium channel, voltage-dependent, L type, alpha 1C subunit	NM_012517	Rn00709287_m1

alcohol for 1 minute, 90% alcohol for 1 minute, and 100% alcohol for 4 minutes. The slides were then placed in histoclear solvent for 10 minutes. Finally, the slides were mounted in DPX and left to dry for an hour. The slides could then be visualized using the light microscope (Zeiss, Axiocam MRc camera) and images were taken using Axiovision software. If, in the images, the SAN artery could be identified, surrounded by a clear region of blue connective tissue containing pale, small, disorganised SAN cells (Fig. 1), these tissue sections were considered appropriate for immunohistochemistry (Figs. 1, 3, 4).

Immunohistochemistry

Slides were fixed in 10% buffered formalin for 30 minutes in a fume cupboard. The slides were then washed in phosphate-buffered saline (PBS) for 10 minutes, thrice. The slides were treated with 0.1% Triton-X100 (1L of PBS mixed with 1mL of Triton-X100) for 30 minutes to permeabilise the plasma membrane. The slides were washed in PBS for 10 minutes, thrice, and blocked with 1% BSA (0.1g of BSA dissolved in 10mL of PBS) for 60 minutes. Sections on each slide were circled with a water-repellent PAP pen

Table 2. Abundance of transcripts between male and female rat hearts. The FDR corrected P values are presented for transcripts showing significant differences with < denoting lower and > denoting higher abundance. '=' sign denotes no change. Female sinoatrial node (FSAN); Female right atrium (FRA); Male sinoatrial node (MSAN); Male right atrium (MRA).

Transcript	FSAN (mean ± SEM)	MSAN (mean ± SEM)	FRA (mean ± SEM)	MRA (mean ± SEM)	FSAN vs FRA	MSAN vs MRA	FRA vs MRA	FSAN vs MSAN
Abcc9	0.274±0.0028	0.261±0.00266	0.334±0.00197	0.386±0.00287	=	0.00245 (<)	=	=
Adora1	0.648±0.00131	0.0775±0.000966	0.0451±0.000574	0.386±0.00126	=	=	0.0407 (<)	=
Adra1a	0.0204±0.000394	0.02±0.000428	0.0208±0.000156	0.0656±0.000314	=	0.0480 (<)	=	=
Adra1d	0.00792±0.000174	0.0121±0.000202	0.00505±7.17E-05	0.0269±0.000134	=	0.0444 (>)	=	=
Adrb2	0.0199±0.000178	0.0199±0.000216	0.0158±0.000194	0.00729±7.84E-05	=	0.0261 (>)	=	=
Atp1a2	0.293±0.00335	0.403±0.00651	0.197±0.00198	0.211±0.00216	0.0328 (>)	0.0154 (>)	=	=
Atp1a3	0.013±0.000406	0.028±0.000665	0.00349±0.000299	0.00071±2.7E-06	0.0273 (>)	2.37E-07 (>)	=	=
Cacna1d	8.73E-05±1.49E-05	2.23E-05±7.7E-06	0.000461±2.02E-05	0.000217±5.73E-06	0.0174 (>)	=	=	0.0416 (>)
Cacna2d3	0.0158±0.000239	0.0117±6.4E-05	0.0169±8.6E-05	0.0153±0.000123	=	0.0298 (<)	=	=
Cacnb1	0.00343±0.000112	0.00252±6.2E-05	0.00151±2.69E-05	0.00107±1.99E-05	0.0247 (>)	0.0181 (>)	=	=
Cacnb3	0.00236±0.000464	0.00301±7.17E-05	0.00179±5.85E-05	0.00116±2.63E-05	=	0.00350 (>)	=	=
Cacng4	0.00368±0.000145	0.00176±1.8E-05	0.00451±0.000106	0.00444±4.83E-05	=	8.26E-05 (<)	=	=
Cacng7	0.0121±0.000174	0.014±0.000158	0.00784±0.000154	0.00575±4.48E-05	0.0443 (>)	0.00269 (>)	=	=
Gja5	0.0245±0.000152	0.0331±0.000488	0.00924±0.000189	0.00501±9.45E-05	0.0443 (>)	2.25E-06 (>)	=	=
HCN1	0.0008±0.000585	0.0247±0.000944	0.00821±0.000633	0.000357±1.85E-05	0.0107 (>)	3.63E-06 (>)	0.00552 (>)	=
HCN4	0.577±0.0145	0.854±0.0168	0.124±0.00672	0.0695±0.00104	0.0121 (>)	5.92E-08 (>)	=	=
Itpr3	0.0215±0.0002	0.0219±0.00024	0.0155±0.00031	0.0119±0.000206	0.0460 (>)	0.00719 (>)	=	=
Kcna5	0.0868±0.0021	0.0567±0.000712	0.0534±0.00139	0.0169±0.000271	=	1.10E-05 (>)	0.00190 (>)	=
Kcnab1	0.00326±8.68E-05	0.00333±8.84E-05	0.00231±6.26E-05	0.00136±2.75E-05	=	0.0339 (>)	=	=
Kcnab2	0.000672±6E-05	0.00039±8.51E-06	8.02E-05±5.04E-06	0.00011±3.39E-06	=	0.0304 (>)	=	=
Kcnb1	0.0873±0.00111	0.098±0.000728	0.0849±0.000524	0.0757±0.000314	=	0.0326 (>)	=	=
Kcne3	0.00243±6.53E-05	0.00228±2.86E-05	0.00132±3.19E-05	0.0008±8.26E-06	=	0.00373 (>)	=	=
Kcnh1	0.000963±3.15E-05	0.000609±2.02E-05	0.000338±5.69E-06	0.000617±2E-05	0.0288 (>)	=	=	=
Kcnj2	0.0235±0.00038	0.0191±0.000286	0.0301±0.000338	0.0336±9.28E-05	=	0.000927 (<)	=	=
Kcnj3	0.999±0.012	0.705±0.007	0.115±0.0113	1.24±0.00932	=	0.000258 (<)	=	0.0351 (>)
Kcnk6	0.0219±0.000152	0.021±0.000193	0.0179±0.000236	0.0138±2.85E-05	=	0.00294 (>)	=	=
Kcnn1	0.00179±2.5E-05	0.00203±3.06E-05	0.00145±3.72E-05	0.00116±1.53E-05	=	0.00624 (>)	=	=
Kcnn3	0.0076±0.000214	0.00835±0.000109	0.0028±9.6E-05	0.00179±4.15E-05	0.0105 (>)	1.12E-05 (>)	=	=
Nkx2-5	0.158±0.00138	0.114±0.00143	0.193±0.00218	0.147±0.00266	=	=	=	0.0386 (>)
Pias3	0.0144±0.00014	0.0163±0.000137	0.012±0.000129	0.01±0.000155	=	0.0470 (>)	=	=
Scn2b	0.00805±0.000215	0.00798±8.98E-05	0.00368±0.000146	0.00177±3.8E-05	0.0236 (>)	0.000468 (>)	=	=
Scn3a	0.00164±4.76E-05	0.00276±4.37E-05	0.000816±2.56E-05	0.000506±1.11E-05	=	2.26E-05 (>)	=	=
Scn3b	0.00507±0.000252	0.00334±7.22E-05	0.00113±6.82E-05	0.00119±2.9E-05	=	0.00227 (>)	=	=
Slc4a1	0.00294±3.13E-05	0.00536±0.000133	0.00299±9.54E-05	0.00192±5.8E-05	=	0.0359 (>)	=	=
Slc4a2	0.0034±0.000409	0.0528±0.000314	0.0462±0.000483	0.0385±0.000203	=	0.00813 (>)	=	=
Slc4a3	0.117±0.00119	0.0905±0.000897	0.156±0.00258	0.126±0.000974	=	0.0165 (<)	=	=
Tgfb1	0.0406±0.000291	0.0363±0.000352	0.0292±0.000147	0.0325±0.000349	0.0163 (>)	=	=	=
Trpc1	0.0253±0.000301	0.0217±0.00011	0.0245±0.000236	0. 0276±0.000175	=	0.0189 (<)	=	=
Trpc3	0.00233±6.52E-05	0.00296±3.93E-05	0.00191±6.2E-05	0.0011±9.81E-06	=	0.000136 (>)	=	=
Trpc4	0.00338±0.000101	0.0059±0.00017	0.000782±7.51E-05	0.000135±7.22E-06	0.00554 (>)	4.96E-05 (>)	=	=
Trpc6	0.00207±6.03E-05	0.00452±0.000167	0.0026±3.41E-05	0.000654±2.36E-05	=	0.00430 (>)	=	=
Trrp5	0.000557±2.53E-05	0.000136±4.75E-06	0.00078±1.83E-05	0.00106±3.87E-05	=	0.00589 (<)	=	=

(Sigma) and then incubated with primary antibody overnight at 4°C. Primary antibodies were in dilutions of 1:50 in 1% BSA in PBS. The slides were then washed in PBS for 10 minutes, thrice, and incubated with secondary antibody at room temperature for 2 hours in dilutions of 1:100 for FITC-conjugates and 1:400 for Cy3-conjugates in 1% BSA in PBS. The slides were washed in PBS for 10 minutes, thrice. Finally, the slides were mounted in Vectashield mounting medium (Vector labs) and cover-slips were sealed with nail varnish.

The primary antibodies used were: anti-HCN4 (Alomone Labs APC-052) raised in rabbit, anti-Cav1.3 (Alomone Labs ACC-005) raised in rabbit, anti-Kir3.1 (Alomone Labs APC-005) raised in rabbit, anti-caveolin3 (BD Transduction Laboratories) raised in mouse and anti-RyR2 (Thermo Scientific) raised in mouse. The secondary antibodies used were: donkey anti-mouse IgG affinity purified Cy3 conjugated absorbed for dual labelling (Millipore); donkey anti-rabbit IgG affinity purified fluorescein conjugated absorbed for dual labelling (Millipore).

Imaging and fluorescence intensity analysis

The Masson's trichrome stained sections were visualised using a light microscope. The sections were

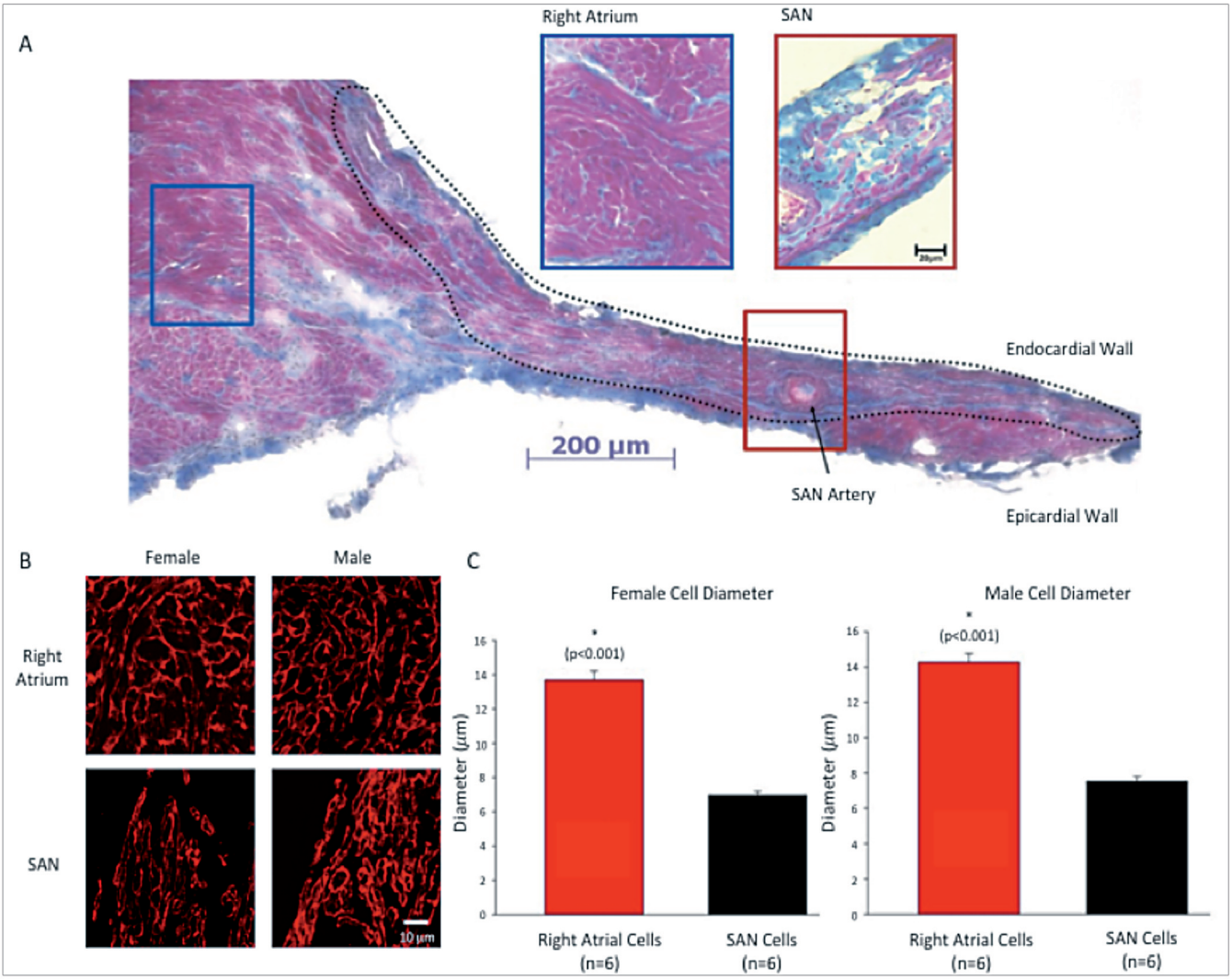

Fig. 1. A. Histology of male rat heart tissue stained with Masson's trichrome, 10x magnification of a cross-section of the RA including the sinoatrial node (cardiomyocytes are purple, connective tissue is blue, nuclei are dark blue). The SAN is outlined by a black dotted line, the endocardial and epicardial wall and sinoatrial node artery are all indicated. Inserts, 63x magnification of RA tissue and SAN. **B.** Caveolin3 immunohistochemistry illustrating the difference between heart cells. SAN cells are smaller and more disorganised than RA cells. Caveolin3 is a marker of both SAN and atrial cell membranes. **C.** Rat heart cell diameters. Graphs showing that female RA cells (13.7±0.53) have significantly larger diameters than female SAN cells (7±0.23), similarly the diameters of male RA cells (14.3±0.5) are significantly larger than SAN cells (7.5±0.26). The diameters of both RA cells and SAN cells were similar between sexes.

imaged using a Axiocam MRc camera (Zeiss) with Axiovision software. A laser scanning confocal microscope (LSM5, Zeiss) was used to visualise the immunofluorescent sections. The fluorophores FITC and Cy3 were used in this case. Appropriate lasers for Cy3 and FITC excitation were used and images were taken using LSM5 Zeiss PASCAL software.

The fluorescent images taken with the confocal microscope were analysed using Volocity software. The intensity of the fluorescence in each image of atrial and/or SAN tissue was semi-quantified and the representative values were averaged. The 'measurements' tab of the voxel spy application within Volocity software enabled non-specific background signal to be excluded when viewing individual images. This was accomplished through selecting 'find objects by intensity (range 10-255)', then selecting 'exclude objects by size (<150 μm)'. T-tests were carried out using SigmaPlot software to determine whether there was a difference in fluorescence intensity between sexes. The graphs were also created using SigmaPlot software.

Computer modelling

Previously published biophysically detailed cell model of the mouse SAN cell AP by Kharche et al. (2011) was used to simulate the dependence of AP duration on ICa,L conductance, gCaL (Kharche et al., 2011).

Results

Histology

Fig. 1A shows a 10x magnification of a cross section of a male rat SAN preparation stained with Masson's trichrome. The insets of Fig. 1A show a 63x magnification of atrial muscle tissue in the blue box and a 63x magnification of SAN tissue in the red box. All other preparations showed similar morphology as in Fig.

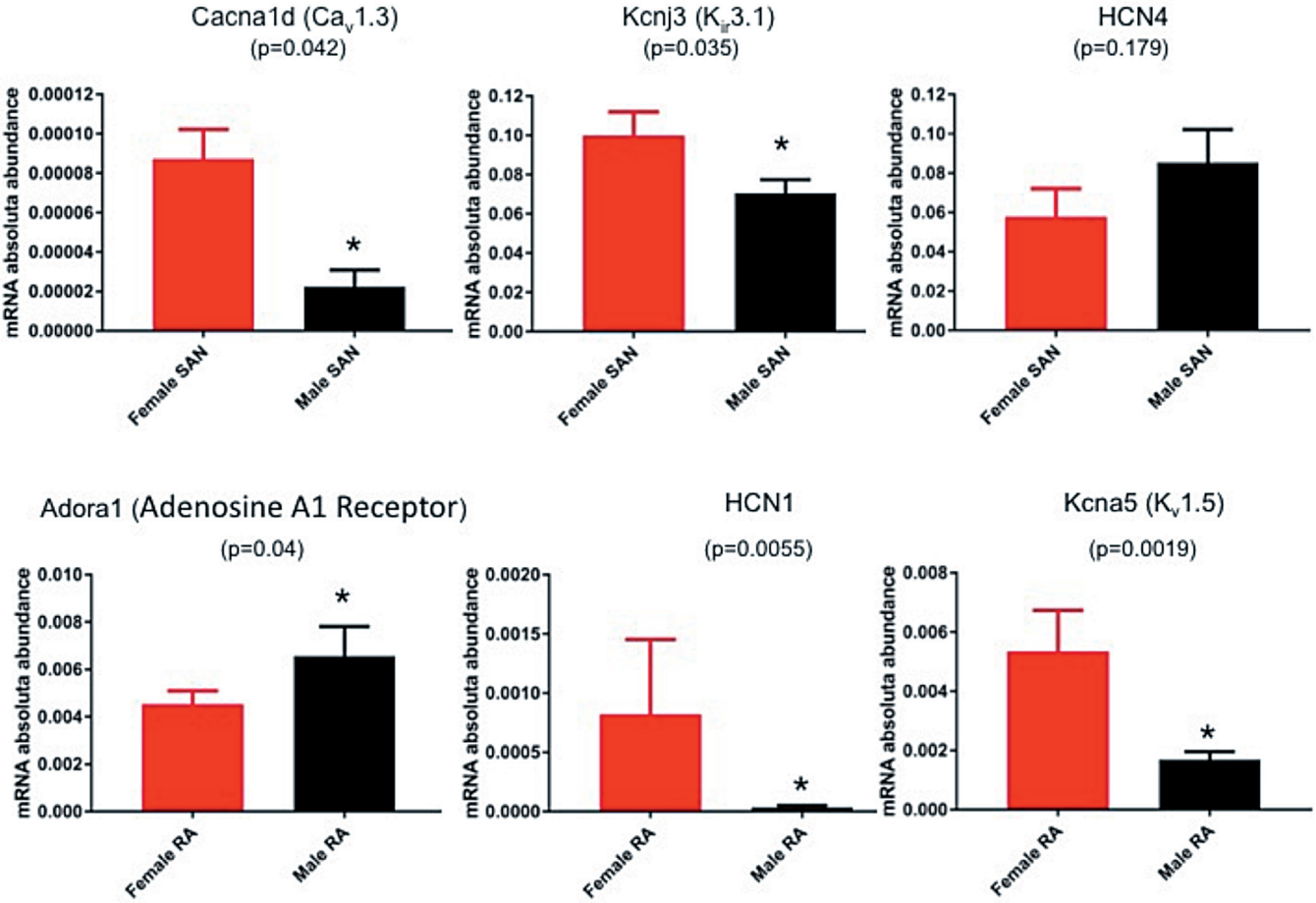

Fig. 2. Graphs illustrating the difference in abundance of messenger RNAs between the sexes' SANs (top) and RAs (bottom). Cancna1d and Kcnj3 levels were higher in female SANs (p=0.042 and p=0.035 respectively). There was no significant difference in HCN4 levels between sexes' SANs (p=0.179). Adora1 levels were higher in male RAs (p=0.04). HCN1 and Kcna5 levels were higher in female RAs (p=0.0055 and p=0.0019 respectively). The data was normalised to the housekeeper gene GAPDH and presented as 2^-ΔCt.

1A. RA cells are darker, larger and more organised than SAN cells. There is an abundance of connective tissue within the SAN compared to surrounding RA muscle. There were no obvious morphological differences in stained SAN preparations between sexes (data not shown). The images determined the approximate location of the SAN in each preparation, thereby establishing which slides from sectioning were most suitable for immunohistochemistry. The histology slides of both sexes had similar microanatomy (Fig. 1).

Cell diameters

RA and SAN cells in male and female rat sections labelled positive for caveolin3 (Fig. 1B), facilitating measurement of RA and SAN cells and showing both

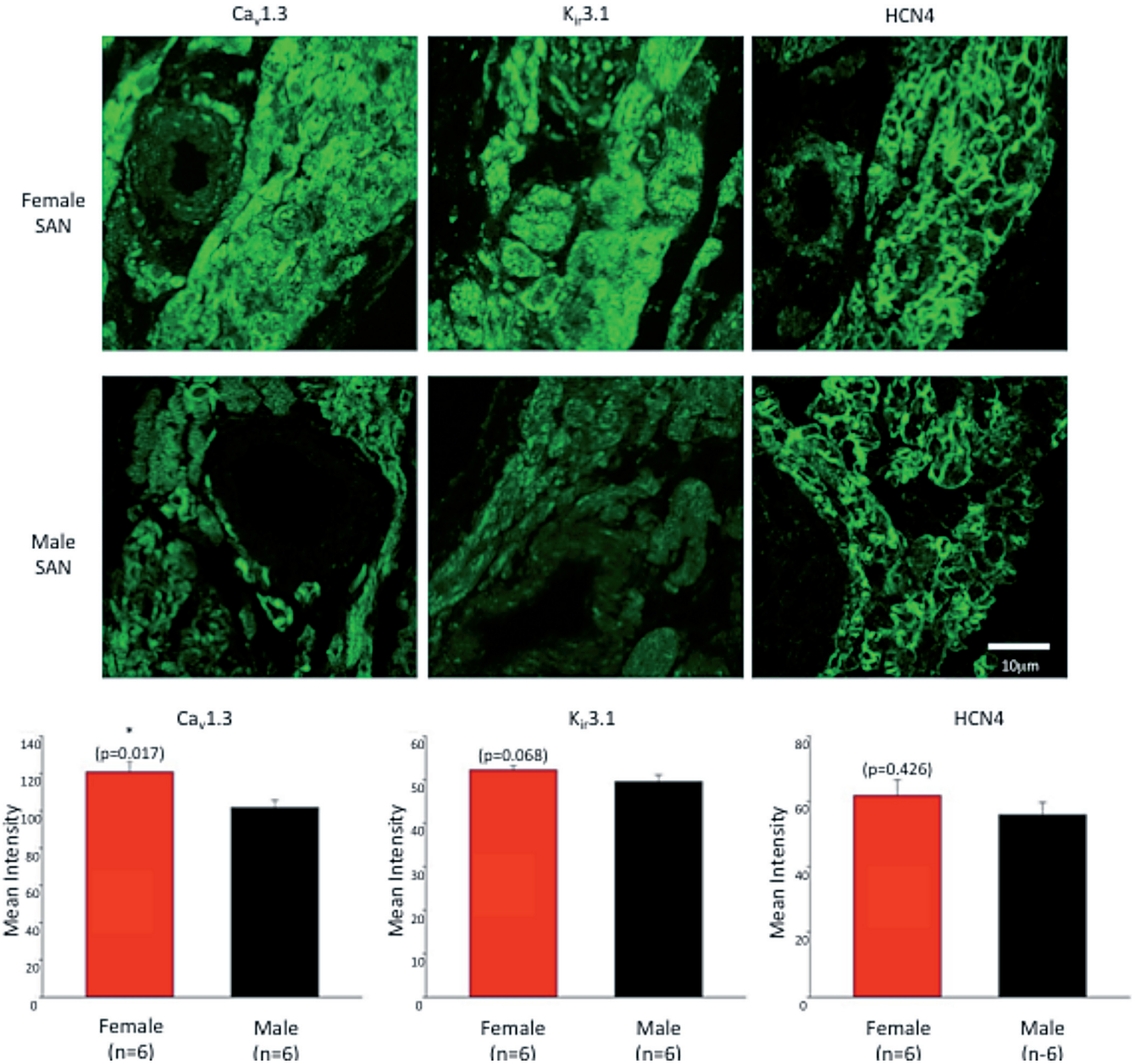

Fig. 3. Top: Immuofluorescence staining of SAN for $Ca_V1.3$ (left column), $K_{ir}3.1$ (middle column), and HCN4 (right) column in females (top row) and males (bottom row). These images show a higher abundance of $Ca_V1.3$ and $K_{ir}3.1$ in the female SAN. There is no difference in abundance of HCN4 between sexes. Bottom: Graphs illustrating the difference in abundance of protein levels between male and female rat SAN. $Ca_V1.3$ levels were higher in females (p=0.017). There was no significant difference in $K_{ir}3.1$ or HCN4 levels between sexes (p=0.068 and p=0.426 respectively).

male and female rat RA cells had significantly larger diameters (Fig. 1C). There was no significant difference in the diameters of RA and SAN cells between sexes (Fig. 1C).

qPCR analysis

96 mRNA transcripts were analysed using TaqMan array microfluidic cards and RealTime StatMiner software (see Table 1). GAPDH was identified as the optimal housekeeping gene to perform normalisation. ΔCt values of the transcripts were inserted into the formula '$2^{-\Delta Ct}$', using Excel software, after which the values were transferred to SigmaPlot software. SigmaPlot was used to perform t-tests and create graphs. Three transcripts ($Ca_v1.3$, $K_{ir}3.1$ and Nkx2-5, a transcription factor) were found to be significantly different between male and female SANs (Fig. 2 and/or Table 2, $P<0.05$). Three were found to be different between male and female RA (Fig. 2 and Table 2, $P<0.05$): Adora1 (an Adenosine A1 receptor) was more abundant in male than female rat RA tissue, whereas, HCN1, and Kcna5 (coding for Kv1.5) were both more abundant in female RA tissue.

14 transcripts were significantly different between female SAN and female RA, 38 between male SAN and male RA (Table 2). Yanni et al. 2011 investigated the difference in abundance of mRNA between male rat RA and SAN in relation to heart failure, which could be compared to the male rat data in this study (Yanni et al., 2011). The comparative abundance of the following transcripts between the RA and SAN of male rats was in accordance with our data: Adra1d, Adrb2, Atp1a2, Atp1a3, Cacnb1, Cacnb3, Cacng4, Cacng7, Gja5, HCN1, HCN4, Itpr3, Kcna5, Kcnb1, Kcne3, Kcnk6, Kcnn1, Kcnn3, Scn2b, Scn3a, Scn3b, Slc4a1, Slc4a2, Trpc3, Trpc4, Trpc6 (Yanni et al., 2011). Chandler et al. (2009) published data for the comparative abundance of mRNA in human SAN and RA and Tellez et al. (2006) published similar data pertaining to rabbits (Lakatta and Sollott, 2002; Tellez et al., 2006). Our data concurs with both papers. Our data also confirms that HCN1 and HCN4 are greater in the SAN in both sexes (Table 2) (Lakatta and Sollott, 2002; Tellez et al., 2006).

Protein expression in female vs. male SAN

SAN cells in male and female rat SAN sections labelled positive for $K_{ir}3.1$, HCN4 and Cav1.3 (Fig. 3) and RyR2 (Fig. 4). Immunoconfocal images were then

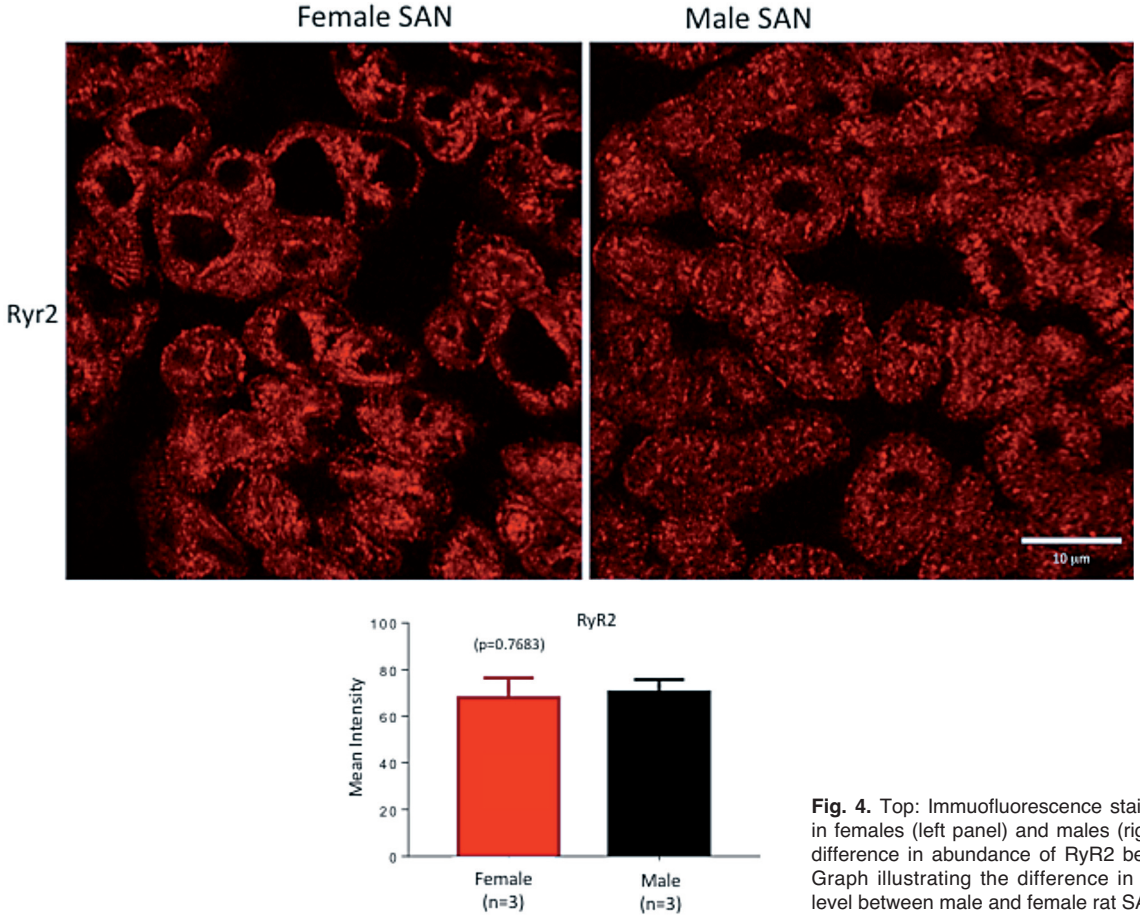

Fig. 4. Top: Immuofluorescence staining of SAN for RyR2 in females (left panel) and males (right panel). There is no difference in abundance of RyR2 between sexes. Bottom: Graph illustrating the difference in abundance of protein level between male and female rat SAN.

analysed using Volocity software and the fluorescence intensities were quantified. $Ca_v1.3$ was more abundant in female SANs and HCN4 expression was not significantly different between sexes (Fig. 3). There was no significant difference in $K_{ir}3.1$ expression between sexes (Fig. 3). There was also no significant difference in RyR2 expression between sexes (Fig. 4).

Extracellular potential recordings

The female rat SAN intrinsic pacemaker rate was found to be significantly higher than that in the male rat SAN (Fig. 5). 5 μM of nifedipine, which blocks $I_{Ca,L}$ ($Ca_v1.3$ and $Ca_v1.2$), was applied to the SAN preparations. The beating rate in male SAN preparations decreased to a significantly greater extent upon exposure to nifedipine compared with female SAN preparations. As a result, the percentage difference between baseline beating rate and beating rate during exposure to nifedipine was significantly greater in male SAN preparations than female SAN preparations (Fig. 5A).

0.1 μM of carbachol, which activates $I_{K,ACh}$, was applied to the SAN preparations. There was no significant difference between sexes in the extent to

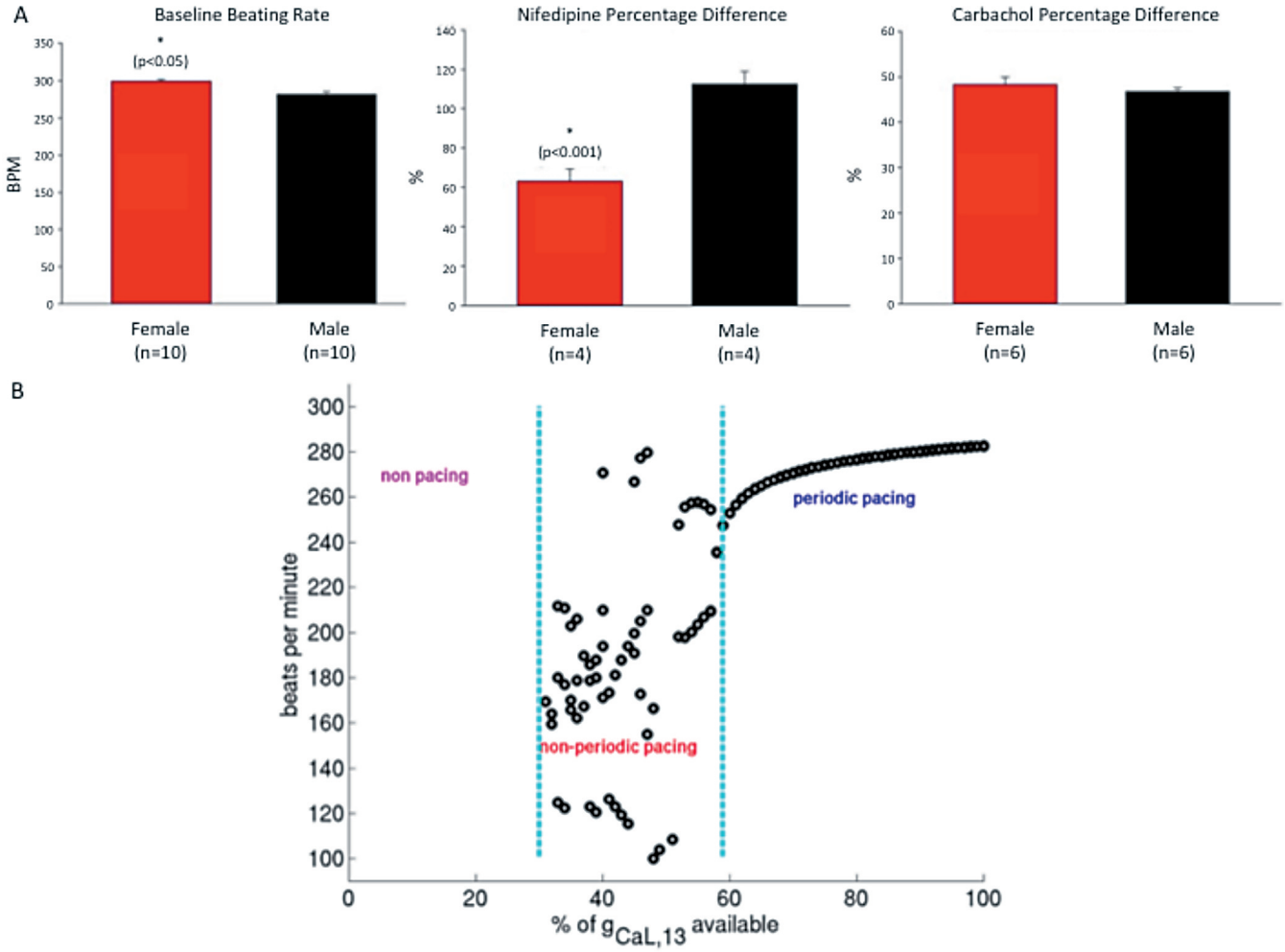

Fig. 5. A. Baseline beating rate of the SAN from both sexes (left). Female rats' baseline heart rate (299±3.01) is significantly higher than male rats' (282±3.99) ($p<0.001$). A t-test and SigmaPlot was used. Nifedipine (middle) and Carbachol (right) extracellular potential recording graphs. Differences were evaluated by t-test with Sigmaplot software. The graphs show that Nifedipine causes the beating rate to decrease more significantly in males (123±6.46) compared with females (176±5.62) ($p<0.001$). There is a greater percentage decrease in beating rate in males (112±6.59) compared with females (63±6.23) ($p<0.001$). There was no significant difference between sexes in the extent to which beating rates decreased under the influence of carbachol; females = 159±4.51; males = 163±2.56; nor was there a significant difference in percentage decrease; females = 48±1.73; males = 47±0.79. **B.** Cell Simulation. Relationship between Cav1.3 L-type calcium current, $I_{CaL,1.3}$, availability and mouse SAN cell model pacemaking behaviour. ICaL availability is represented by a fraction of I_{CaL} conductance. When $I_{CaL,1.3}$ was available to between 0 to 30% of its control value the model was non-pacemaking and did not produce APs. When $I_{CaL,1.3}$ was available between 30 and 60%, non-periodic pacemaking was observed. At values of $I_{CaL,1.3}$ above 60%, periodic pacemaking was observed. In the periodic pacemaking range, the pacemaking rate increased as $I_{CaL,1.3}$ availability was increased.

which the rates decreased upon exposure to carbachol. Therefore, there was no significant difference between sexes in the percentage difference between baseline beating rate and beating rate upon exposure to carbachol (Fig. 5A).

The computer modelling results are illustrated in Fig. 5B. The model shows stable pacemaking as long as more than 60% g_{CaL} was available. When only 30% to 60% gCaL was available, the model produced aperiodic APs representing arrhythmia. When g_{CaL} was set to less than 30% of its control value, pacemaking was arrested in the model.

Discussion

Our results demonstrate, for the first time, significant sex-based differences in the key pacemaker ion channel expression (especially $Ca_v1.3$ and $K_{ir}3.1$) within the SAN and its effect on the intrinsic SAN function. Could the differences in $Ca_v1.3$ and/or $K_{ir}3.1$ expression explain females' propensity for SSS as shown in epidemiological studies? Recent work showed that targeting G protein-gated K^+ ($I_{K,ACh}$) channels effectively rescues SSS of $Ca_v1.3^{-/-}$ mice (Mesirca et al., 2016).

The morphology of male and female rat SANs are consistent with characteristics recorded in literature (Dobrzynski et al., 2013). SAN cells are surrounded by connective tissue with high collagen content, which stained blue with Masson's tichrome (Fig. 1A) (De Mazière et al., 1992). SAN cell diameter ranges between 5-10 μm and atrial cell diameter is between 15-20 μm in the human, dog, rabbit, guinea-pig, cat, monkey, and pig (Boyett et al., 2000; Dobrzynski et al., 2013). The caveolin3 labelling showed that RA cells were significantly larger than SAN cells in both sexes (Fig. 1B,C). These images also showed that RA and SAN cell diameters were similar between sexes, confirming that male and female SANs are morphologically similar. The arrangement of the SAN cells is 'interweaving' compared with the organised RA cells (Fig. 1A) (Bleeker et al., 1980). The SAN cells are paler than RA cells (Fig. 1A), thought to be due to their lower content of myofilaments, mitochondria and sarcoplasmic reticulum (James et al., 1966; Boyett et al., 2000; Dobrzynski et al., 2013). The Masson's trichrome stained SANs showed no morphological differences between sexes (data not shown).

The higher abundance of HCN4 and $Ca_v1.3$ channels in SAN cells than in RA cells has been previously recognised (Mangoni and Nargeot, 2008). A channel isoform switch occurs moving from the SAN to the atrial muscle, where $Ca_v1.3$ is substituted by $Ca_v1.2$ (Tellez et al., 2006). The increased abundance of HCN4 and $Ca_v1.3$ channels is a characteristic of cells capable of automaticity (Mangoni and Nargeot, 2008). Raised HCN4 and $Ca_v1.3$ in SAN cells also explains why fluorescent labelling of these channels caused the location of the SAN to be clearly distinct from the atrial muscle. $I_{K,ACh}$ is more abundant in the SAN than in RA, reflecting how the abundance of $K_{ir}3.1$ mRNA tends to increase from RA to SAN cells. However, the difference in abundance of $K_{ir}3.1$ mRNA between SAN and RA cells did not reach statistical significance (Tellez et al., 2006). Western blotting has also shown a similar abundance of $K_{ir}3.1$ protein in the atrium and intercaval region (containing the SAN) in rat hearts (data not shown) (Lakatta and Sollott, 2002). This accounts for difficulties distinguishing the SAN from the atrial muscle when $K_{ir}3.1$ channels were labelled during immunohistochemistry.

TaqMan array microfluidic card analysis detected the expression of three transcripts that differed significantly between female and male rat SANs; Cacna1d (coding for $Ca_v1.3$), Kcnj3 (coding for $K_{ir}3.1$), and Nkx2-5. These three transcripts were more abundant in females. Interestingly, HCN4 mRNA tended towards being more abundant in males (Fig. 2).

Nkx2-5 is expressed in the heart and plays a role in heart development and function (Zhou et al., 2015). Reports indicate that Nkx2-5 is mainly not expressed in the SAN (Wiese et al., 2009). Nkx2-5 is thought to be repressed by the Shox2 homeodomain transcription factor, thereby allowing differentiation of cardiac pacemaker cells (Espinoza-Lewis et al., 2009). It is unclear why Nkx2-5 would be more abundant in the female SAN. Perhaps, this higher abundance of Nkx2-5 could explain female propensity for SSS; Ye et al. 2015 conducted an experiment wherein Shox2 deletion in the Nkx2-5 expressing tail portion of the SAN resulted in SSS (Ye et al., 2015).

$Ca_v1.3$ and $K_{ir}3.1$ channels at protein level were expected to be more abundant in female SANs, thereby providing an explanation for some of the differences observed in SAN function between sexes. Increased abundance of $Ca_v1.3$ could increase the rate of diastolic depolarisation during phase 4 of the female AP. Increased abundance of $K_{ir}3.1$ could generate a greater $I_{K,Ach}$, eventually causing more negative hyperpolarization and reduced intrinsic beating rate in females (Mesirca et al., 2013).

Semi-quantitative fluorescence intensity analysis was performed on images labelled for $Ca_v1.3$, $K_{ir}3.1$, HCN4 and RyR2. The analysis showed $Ca_v1.3$ channels were significantly raised in females. There was no significant difference in HCN4 channel levels between sexes (but there was a trend towards higher expression in females). There was also no significant difference in $K_{ir}3.1$ channel levels between sexes, which was expected to be higher in females. However, levels of $K_{ir}3.1$ channels being greater in females tended towards significance ($p=0.068$). In addition, there was no significant difference in the expression of RyR2 protein between sexes.

Baseline beating rates in rat SAN preparations of both sexes was previously recorded by Barrett et al.

(1998). The mean SAN beating rate recorded was 295±11 BPM (Barrett et al., 1998). The mean beating rate of female rat SAN preparations from our study lies within this value and the male rat SAN preparations' mean beating rate overlaps with this value (Fig. 5). Mangoni et al. (2003) found that inactivation of $Ca_v1.3$ caused slowing of pacemaker activity, which suggests that $Ca_v1.3$ channel abundance influences pacing rate (Mangoni et al., 2003). Therefore, raised $Ca_v1.3$ expression in the female SAN provides an explanation for the greater baseline beating rate.

The application of 5 μM nifedipine to SAN preparations in this study decreased the beating rate in both sexes. However, the decrease in beating rate was more significant in male SAN preparations compared with females' (Fig. 5). Immunofluorescence semi-quantitative analysis showed a greater abundance of Cav1.3 in female SAN cells compared with males' (Fig. 3).

Jones et al. (2007) performed similar experiments on guinea pig SAN preparations and found a declining abundance of $Ca_v1.2$ in the SAN as it ages and a correspondingly heightened sensitivity to nifedipine (Jones et al., 2007). Following this logic, nifedipine sensitivity may be greater in male SAN preparations compared with female because $Ca_v1.3$ is less abundant in male SANs. This is reflected in the modelling study where the $Ca_v1.3$ in females could be represented as 100% while that in males would have a value between 60% to 100%. The female SAN cells may require a larger suppression of $Ca_v1.3$ prior to arrhythmia onset. In contrast, a smaller amount of reduction in g_{CaL} would be sufficient to make the pacemaking arrhythmic (i.e. aperiodic). The modelling demonstrates the higher propensity of males, in comparison to females, to SAN arrhythmia based on $Ca_v1.3$ alterations (Fig. 5).

$K_v1.5$ channels are thought to be expressed exclusively in the atria and are responsible for $I_{K,ur}$, which contributes to early repolarisation (Schmitt et al., 2014). $K_v1.5$ channel mutations are associated with familial atrial fibrillation (AF) and early-onset lone AF (Schmitt et al., 2014). Remodelling of $K_v1.5$ channels in cases of AF has produced equivocal results, both no change and downregulation has been reported (Schmitt et al., 2014; Algalarrondo and Nattel, 2016). $I_{K,ur}$ inhibition shortens AP duration in sinus rhythm, which is thought to be due to a resultant elevated plateau potential, allowing increased $I_{K,r}$ and $I_{K,s}$ activation, leading to accelerated repolarisation (Schmitt et al., 2014). Interestingly, $I_{K,ur}$ inhibition prolongs AP duration in AF, as plateau potentials fail to elevate to the same extent (Schmitt et al., 2014). Incidence and prevalence of AF is lower in women than it is in men (Algalarrondo and Nattel, 2016). Could higher expression of $K_v1.5$ in female's atria as observed in our study be protective? A better understanding of changes in K^+ channels will help clinicians to appreciate arrhythmia mechanisms and facilitate personalized management of arrhythmias in patients with heart disease.

Conclusion

Male and female SAN preparations exhibited significant molecular differences, providing an explanation for why functional differences have been observed between the SANs of the sexes in both rats and humans. qPCR analysis showed Cacnad1, Kcnj3 and Nkx2-5 mRNA levels to be raised in female rats. Semi-quantitative analysis of immunohistochemistry showed $Ca_v1.3$ ion channel expression was also raised in females. Nifedipine application to SAN preparations produced a greater reduction in beating rate in males, indicating that male SANs are more sensitive to L-type calcium channel blocking effects of nifedipine, likely due to their reduced expression of $Ca_v1.3$. These data could explain why females are more prone to certain arrhythmias and less prone to others.

Future work should concentrate on sex differences related to age-dependent changes in the structure of the SAN at the macroscopic, microscopic, molecular biology and functional levels, including human studies. As clinical practice enters the era of personalized 'precision medicine', sex is a key biological variable that has been overlooked and may be a simple and high-yield first step towards individualized care. A review by Keller and Howlett (2016) elegantly described that the number of ventricular myocytes declines with age through apoptosis in men but not in women (Keller and Howlett, 2016). Therefore, further research into aging myocardium and cardiac conduction system in both sexes is needed.

Acknowledgements. We thank Professor Mark R Boyett on his expert advice on the work described in this manuscript and Dr. James O. Tellez for carrying out the qPCR experiments. This study was supported by the British Heart Foundation (BHF Project Grant no. PG/17/32/32987). This work was carried out within the framework of Tomsk Polytechnic University Competitiveness Enhancement Program.

Author contributions statement. HD was the project leader and supervised UD, MP, BB, SK, SL, OF, YZ, AD, AJA, JY. UD carried out qPCR analysis and all the methods (apart from qPCR and computer modelling) and together with HD prepared this manuscript. SRK carried out the computer modelling. MP, BB, AJA assisted with histology, immunohistochemistry and imaging. OF and YZ helped with optimisation of immunohistochemistry. MM and UM provided hearts for qPCR experiments. AC provided advice on the manuscript. AD helped with data interpretation. JY oversaw qPCR analysis and assisted with functional experiments. SL helped with functional experiments. All authors revised the manuscript.

Conflict of interest statement. The authors declare that the submitted work was not carried out in the presence of any personal, professional, or financial relationships that could potentially be construed as a conflict of interest.

References

Algalarrondo V. and Nattel S. (2016). Potassium channel remodeling in heart disease. Card. Electrophysiol. Clin. 8, 337-347.

Barrett C., Bolter C. and Wilson S. (1998). The intrinsic rate response of the isolated right atrium of the rat, *Rattus norvegicus*. Comp. Biochem. Physiol. 120, 391-397.

Bleeker W., Mackaay A., Masson-Pevet M., Bouman L. and Becker A. (1980). Functional and morphological organization of the rabbit sinus node. Circ. Res. 46, 11-22.

Boyett M., Honjo H. and Kodama I. (2000). The sinoatrial node, heterogenous pacemaker structure. Cardiovasc. Res. 47, 658-687.

Burke J.H., Goldberger J.J., Ehlert F.A., Kruse J.T., Parker M.A. and Kadish A.H. (1996). Gender differences in heart rate before and after autonomic blockade: evidence against an intrinsic gender effect. Am. J. Med. 100, 537-543.

Chandler N.J., Greener I.D., Tellez J.O., Inada S., Musa H., Difrancesco D., Baruscotti M., Longhi R., Anderson R.H., Billeter R., Sharma V., Sigg D.C., Boyett M.R. and Dobrzynski H. (2009). Molecular architecture of the human sinus node: insights into the function of the cardiac pacemaker. Circulation 119, 1562-1575.

De Mazière A., van Ginneken A., Wilders R., Jongsma H. and Bouman L. (1992). Spatial and functional relationship between myocytes and fibroblasts in the rabbit sinoatrial node. J. Mol. Cell Cardiol. 24, 567-578.

Dobrzynski H., Marples D., Musa H., Yamanushi T.T., Henderson Z., Takagishi Y., Honjo H., Kodama I. and Boyett M.R. (2001). Distribution of the muscarinic K+ channel proteins Kir3.1 and Kir3.4 in the ventricle, atrium, and sinoatrial node of heart. J. Histochem. Cytochem. 49, 1221-1234.

Dobrzynski H., Anderson R., Atkinson A., Borbas Z., D'Souza A., Fraser J.F., Inada S., Logantha S.J., Monfredi O., Morris G.M., Moorman A.F., Nikolaidou T., Schneider H., Szuts V., Temple I.P., Yanni J. and Boyett M.R. (2013). Structure, function and clinical relevance of the cardiac conduction system including the atrioventricular ring and outflow tract tissues. Pharmacol. Ther. 139, 260-288.

Espinoza-Lewis R.A., Yu L., He F., Liu H., Tang R., Shi J., Sun X., Martin J.F., Wang D., Yang J. and Chen Y. (2009). Shox2 is essential for the differentiation of cardiac pacemaker cells by repressing Nkx2-5. Dev. Biol. 327, 376-385.

James T., Sherf L., Fine G. and Morales A. (1966). Comparative ultrastructure of the sinus node in man and dog. Circulation 34, 139-163.

Jones S., Boyett M. and Lancaster M. (2007). Declining into failure: The age-dependent loss of the L-type calcium channel within the sinoatrial node. Circulation 115, 1183-1190.

Keller K.M. and Howlett S.E. (2016). Sex differences in the biology and pathology of the aging heart. Can J. Cardiol. 32, 1065-1073.

Kharche S., Yu J., Lei M. and Zhang H. (2011). A mathematical model of action potentials of mouse sinoatrial node cells with molecular bases. Am. J. Physiol. Heart Circ. Physiol. 301, H945-963.

Kharche S.R., Vigmond E., Efimov I.R. and Dobrzynski H. (2017). Computational assessment of the functional role of sinoatrial node exit pathways in the human heart. PLoS One 12, e0183727.

Lakatta E.G. and Sollott S.J. (2002). Perspectives on mammalian cardiovascular aging: humans to molecules. Comp Biochem. Physiol. A Mol. Integr. Physiol. 132, 699-721.

Mangoni M. and Nargeot J. (2008). Genesis and regulation of the heart automaticity. Physiol. Rev. 88, 919-982.

Mangoni M., Couette B., Bourinet E., Platzer J., Reimer D., Striessnig J. and Nargeot J. (2003). Functional role of L-type Cav1.3 Ca2+ channels in cardiac pacemaker activity. Proc. Natl. Acad. Sci. 100, 5543-5548.

Mesirca P., Bidaud I. and Mangoni M. (2016). Rescuing cardiac automaticity in L-type Cav1.3 channelopathies and beyond. J. Physiol. 594, 5869-5879.

Mesirca P., Marger L., Toyoda F., Rizzetto R., Audoubert M., Dubel S., Torrente A.G., Difrancesco M.L., Muller J.C., Leoni A.L., Couette B., Nargeot J., Clapham D.E., Wickman K. and Mangoni M.E. (2013). The G-protein–gated K+ channel, IKACh, is required for regulation of pacemaker activity and recovery of resting heart rate after sympathetic stimulation. J. Gen. Physiol. 142, 113-126.

Mesirca P., Torrente A.G. and Mangoni M.E. (2015). Functional role of voltage gated Ca2+ channels in heart automaticity. Front. Physiol. 6, 19.

Morris G., D'Souza A., Dobrzynski H., Lei M., Choudhury M., Billeter R., Kryukova Y., Robinson R.B., Kingston P.A. and Boyett M.R. (2013). Characterisation of a right atrial subsidiary pacemaker and acceleration of the pacing rate by HCN over-expression. Cardiovasc. Res. 100, 160-169.

Nowak B., Misselwitz B., Erdogan A., Funck R., Irnich W., Israel C.W., Olbrich H.G., Schmidt H., Sperzel J. and Zegelman M. (2010). Do gender differences exist in pacemaker implantation? - Results of an obligatory external quality control program. Europace 12, 210-215.

Peters R.W. and Gold M.R. (2004). The influence of gender on arrhythmias. Cardiol. Rev. 12, 97-105.

Rubenstein J., Schulman C., Yurchak P. and Desanctis R. (1972). Clinical spectrum of the sick sinus syndrome. Circulation 46, 5-13.

Sanjeev S. and Karpawich P.P. (2005). Developmental changes in sinus node function in growing children: an updated analysis. Pediatr. Cardiol. 26, 585-588.

Schmitt N., Grunnet M. and Olesen S.P. (2014). Cardiac potassium channel subtypes: new roles in repolarization and arrhythmia. Physiol. Rev. 94, 609-653.

Tadros R., Ton A.T., Fiset C. and Nattel S. (2014). Sex differences in cardiac electrophysiology and clinical arrhythmias: epidemiology, therapeutics, and mechanisms. Can. J. Cardiol. 30, 783-792.

Taneja T., Mahnert B.W., Passman R., Goldberger J. and Kadish A. (2001). Effects of sex and age on electrocardiographic and cardiac electrophysiological properties in adults. Pacing Clin. Electrophysiol. 24, 16-21.

Tellez J.O., Dobrzynski H., Greener I.D., Graham G.M., Laing E., Honjo H., Hubbard S.J., Boyett M.R. and Billeter R. (2006). Differential expression of ion channel transcripts in atrial muscle and sinoatrial node in rabbit. Circ. Res. 99, 1384-1393.

Wiese C., Grieskamp T., Airik R., Mommersteeg M.T., Gardiwal A., de Gier-de Vries C., Schuster-Gossler K., Moorman A.F., Kispert A. and Christoffels V.M. (2009). Formation of the sinus node head and differentiation of sinus node myocardium are independently regulated by Tbx18 and Tbx3. Circ. Res. 104, 388-397.

Yanni J., Tellez J.O., Maczewski M., Mackiewicz U., Beresewicz A., Billeter R., Dobrzynski H. and Boyett M.R. (2011). Changes in ion channel gene expression underlying heart failure-induced sinoatrial node dysfunction. Circ. Heart Fail. 4, 496-508.

Ye W., Wang J., Song Y., Yu D., Sun C., Liu C., Chen F., Zhang Y.,

Wang F., Harvey R.P., Schrader L., Martin J.F. and Chen Y. (2015). A common Shox2–Nkx2-5 antagonistic mechanism primes the pacemaker cell fate in the pulmonary vein myocardium and sinoatrial node. Development 142, 2521-2532.

Zhou M., Liao Y. and Tu X. (2015). The role of transcription factors in atrial fibrillation. J. Thorac. Dis. 7, 152-158.

Accepted April 10, 2019.